Carbohydrate Polymers 110 (2014) 173–182

Contents lists available at ScienceDirect

Carbohydrate Polymers

journal homepage: www.elsevier.com/locate/carbpol

Characterization and cytocompatibility of an antibiotic/chitosan/cyclodextrins nanocoating on titanium implants

Monica Mattioli-Belmonte[a], Stefania Cometa[b], Concetta Ferretti[a], Roberta Iatta[c], Adriana Trapani[d], Edmondo Ceci[c], Mirella Falconi[e], Elvira De Giglio[f,*]

[a] Department of Clinical and Molecular Sciences, Università Politecnica delle Marche, Via Tronto 10/A, 60126 Ancona, Italy
[b] Jaber Innovation s.r.l., Via Calcutta 8, 00100 Roma, Italy
[c] Department of Veterinary Medicine, University of Bari Aldo Moro, Str. Prov. per Casamassima Km 3, Valenzano (BA), Italy
[d] Department of Pharmacy-Drug Sciences, University of Bari Aldo Moro, Via E. Orabona 4, 70126 Bari, Italy
[e] Department of Biomedical and Neuromotor Sciences, University of Bologna, Via Irnerio 48, 40126 Bologna, Italy
[f] Department of Chemistry, University of Bari Aldo Moro, Via E. Orabona 4, 70126 Bari, Italy

ARTICLE INFO

Article history:
Received 27 December 2013
Received in revised form 24 March 2014
Accepted 26 March 2014
Available online 8 April 2014

Keywords:
Chitosan nanoparticles
Cyclodextrins
Ciprofloxacin
Orthopaedic infections
Cytocompatibility
Gene expression

ABSTRACT

A novel ciprofloxacin loaded chitosan nanoparticle-based coating onto titanium substrates has been developed and characterized to obtain an orthopaedic implant surface able to in situ release the antibiotic for the prevention of post-operative infections. Ciprofloxacin loaded chitosan nanoparticles were obtained using the combination of sulfobutyl ether-beta-cyclodextrin and gamma-cyclodextrin. The resulting nanoparticulate system was characterized by TEM, HPLC and XPS. Particle size was in the range 426–552 nm and zeta potential values were around +30 mV. This antibacterial coating was able to in vitro inhibit two nosocomial *Staphylococcus aureus* strains growth, with a reduction of about 20 times compared to controls. No impairment in MG63 osteoblast-like cells viability, adhesion and gene expression were detected at 48 h, 7 and 14 days of culture. Overall, the investigated coating represents a promising candidate for the development of a new antibiotic carrier for titanium implants.

© 2014 Elsevier Ltd. All rights reserved.

1. Introduction

Infections caused by nosocomial bacteria still remain a major challenge in orthopaedic surgery. Data reported by the Nosocomial Infection National Surveillance Scheme (NINNS) indicated that in hip replacement surgery over 50% of superficial and deep wound infections detected during the in-patient stay were due to *Staphylococcus aureus* (Cooke et al., 2000), which are also capable to produce a biofilm protecting the microbial populations from host immune defence. Today, in particular for orthopaedic implant associated infections, different strategies for the local delivery of antibiotics have been developed: thin biodegradable polymer coatings (Buchholz & Engelbrecht, 1970; Gollwitzer et al., 2003; Lucke et al., 2003), biodegradable polypeptide multilayer nanofilms (Li, Ogle, Jiang, Hagar & Li, 2010); biomimetic hydroxyapatite coatings (Brohede et al., 2009); modification of titanium implant surfaces by covalently bonded antibiotics (Jose, Antoci, Zeiger, Wickstrom, & Hickok, 2005) or linkage through a self-assembled monolayer (Noreen, Hickok, & Shapiro, 2012), etc. Limited investigation has been, indeed, devoted to the use of hydrogels carrying antimicrobial agents as possible coatings of metal implants (Giammona et al., 2010; Romano, Giammona, Giardino, & Meani, 2011). Certainly, hydrogel networks, due to their specific ability to entrap high water amounts, represent an ideal candidate for a sustained antibiotic delivery system. We already reported the electrosynthesis of hydrogel coatings onto titanium substrates (De Giglio, Cometa, Satriano, Sabbatini, & Zambonin, 2009; De Giglio et al., 2010) that, due to their swelling capabilities, were able to entrap and release antibacterial agents, demonstrating an interesting activity against microorganisms (Cometa, Iatta, Ricci, Ferretti, & De Giglio, 2013; De Giglio, Cometa, et al., 2011; De Giglio et al., 2013).

Biodegradable polymeric nanoparticles (NPs) could be also used as alternative delivery systems to achieve antibacterial coatings for titanium implants. In this context, chitosan, a cationic polysaccharide obtained from the alkaline deacetylation of chitin, is particularly attractive for pharmaceutics applications (Agnihotri,

* Corresponding author. Tel.: +39 080 5442021; fax: +39 080 5442021.
E-mail addresses: m.mattioli@univpm.it (M. Mattioli-Belmonte), stefania.cometa@virgilio.it (S. Cometa), c.ferretti@univpm.it (C. Ferretti), iroberta@hotmail.com (R. Iatta), adriana.trapani@uniba.it (A. Trapani), edmondo.ceci@uniba.it (E. Ceci), mirella.falconi@unibo.it (M. Falconi), elvira.degiglio@uniba.it (E. De Giglio).

http://dx.doi.org/10.1016/j.carbpol.2014.03.097
0144-8617/© 2014 Elsevier Ltd. All rights reserved.

Mallikarjuna, & Aminabhavi, 2004; Paul & Sharma, 2000). Several reasons induce to adopt chitosan as a coating layer for titanium implants. When chitosan is protonated in acid solutions, its positive charges can promote cell adhesion (Bumgardner et al., 2003), and several studies already reported its ability to improve specific cell line growth, such as osteoblasts (Amaral, Sampaio, & Barbosa, 2006; Heinemann, Heinemann, Bernhardt, Worch, & Hanke, 2008; Lahiji, Sohrabi, Hungerford, & Frondoza, 2000). Because of its excellent biocompatibility, biodegradability, nontoxicity and adsorption properties, it has been widely used in biomedical area, such as haemostatic agent (Busilacchi, Gigante, Mattioli-Belmonte, Manzotti, & Muzzarelli, 2013; Thatte, Zagarins, Khuri, & Fischer, 2004) or as drug vehicle (Park, Saravanakumar, Kim, & Kwon, 2010). Promising results have also been obtained when chitosan has been used to formulate NPs that showed high loading and good delivery ability of various compounds like dopamine (De Giglio, Trapani, Cafagna, Sabbatini, & Cometa, 2011; Trapani et al., 2011) or antibiotics (Motwani et al., 2008; Ventura et al., 2008, 2011). In this respect, we have previously demonstrated that chitosan nanoparticles, obtained using sulfobutyl ether-β-cyclodextrin, were able to vehicle ciprofloxacin, thus providing an effective inhibition of *S. aureus* and *P. aeruginosa* growth (De Giglio et al., 2012).

In this work, we developed a novel chitosan nanoparticle based coating on titanium as ciprofloxacin (CIP) delivery system, exploiting for the first time the joint action of sulfobutyl ether-β-cyclodextrin (SBE_{7m}-β-CD) and γ-cyclodextrin (γ-CD). In literature, the interaction between the antibiotic CIP and CDs has been widely explored as reported for the natural β-CD (Chandran, Shirwaikar, Sarala, & Devi Kiron, 2010) and the derivative methyl-β-CD (Blanchemain et al., 2011). CIP was chosen for its broad antimicrobial spectrum associated with no genotoxic effects (Herbold, Brendler-Schwaab, & Ahr, 2001) and its common use in orthopaedic local delivery systems (De Giglio, Cometa, et al., 2011; Mattioli-Belmonte et al., 2010; Sansone et al., 2009). Chemico-physical characterization, antibiotic release ability, in vitro antibacterial activity against different nosocomial strains as well as the MG63 osteoblast-like cells proliferation, cytoskeletal organization and gene expression were extensively investigated in this study.

2. Materials and methods

2.1. Materials

Chemicals, listed below, were obtained from commercial sources and used without further modification. Chitosan hydrochloride (UP CL 113, *Mw* 110 kDa, deacetylation degree 75–90% according to manufacturer instructions) was obtained from Pronova Biopolymer (Norway). Titanium foils (thickness 0.25 mm) and ciprofloxacin hydrochloride (*Mw* 385.82 Da) were purchased from Sigma–Aldrich (Italy). Sulfobutyl ether-β-cyclodextrin sodium salt (SBE_{7m}-β-CD, *Mw* 2163 Da, average substitution degree = 6.40) and γ-cyclodextrin (γ-CD, *Mw* 1320 Da) were purchased from CyDex, Inc. (USA) and Wacker-Chemie GmbH (Italy), respectively. CDs were kept in a desiccator until use. Ultrapure water, by Carlo Erba (Italy) was used throughout the study. All other chemicals were reagent grade.

2.2. Preparation of chitosan nanoparticles-based coatings onto titanium substrates

A modified ionic gelation method was adopted to formulate chitosan nanoparticles (CSNPs) in the presence and in the absence of CIP. Briefly, for the preparation of chitosan nanoparticles loaded with CIP (hereafter mentioned as "CIP-loaded CSNPs"), two separate inclusion complexes (i.e., SBE-β-CD/CIP and γ-CD/CIP) were prepared. In order to maintain the molar ratio stoichiometry 1:1 (CD:CIP), for the SBE-β-CD/CIP one, the concentrations were equal to 4.50 mg/mL and 0.81 mg/mL, respectively, whereas for γ-CD and CIP, the concentrations were set at 4.50 mg/mL and 1.30 mg/mL, respectively. An aliquot of 0.2 mL of the complex γ-CD/CIP was firstly mixed with 1.5 mL of chitosan and, in the following step, the use of 0.7 mL of the complex SBE-β-CD/CIP allowed the formation of NPs via a non-covalent crosslinking. Chitosan nanoparticles without CIP (i.e., "unloaded CSNPs") were formulated following the same protocol in the absence of the antibiotic. To promote the adsorption of an additional amount of antibiotic, a further aliquot of the complex γ-CD/CIP was incubated with the final CIP-loaded CSNPs suspension for 3 h at room temperature without any stirring, obtaining the so-called "CIP-enriched CSNPs". The CIP-enriched CSNPs coatings were deposited onto titanium sheets by casting on each sample 1.4 mg of CSNPs, which had previously adsorbed 1.5×10^{-2} mL of the γ-CD/CIP complex. On the other hand, the unloaded CSNPs coatings were obtained by casting 1.4 mg of unloaded CSNPs, which had previously adsorbed 1.5×10^{-2} mL of the aqueous solution of γ-CD (4.5 mg/mL). The resulting coatings were taken as control during biological experiments. Titanium sheets were coated on both sides and were oven-dried at 40 °C.

2.3. Chemico-physical characterization of nanoparticles

Particle size and polydispersity index (PI) of all tested NPs were determined in ultrapure water by Photon Correlation Spectroscopy (PCS) using a Zetasizer NanoZS (ZEN 3600, Malvern, UK). The determination of the ζ-potential was performed using laser Doppler anemometry with 1 mM KCl as carrier.

TEM nanoparticles characterization. Morphological evaluation of unloaded CSNPs and CIP-loaded CSNPs was performed with transmission electron microscope (TEM). 5 μl of each sample solution was dropped on carbon/formvar grids and air dried. Samples were counterstained with 2% (w/v) phosphotungstic acid, air dried and analysed by a TEM Philips CM10 (FEI, Eindhoven, the Netherlands). Images were recorded using a Megaview III digital camera (FEI).

2.4. X-ray photoelectron spectroscopy (XPS) analysis

XPS has been exploited for the surface characterization of all the investigated nanoparticle systems. XPS spectra were obtained with a Thermo VG Thetaprobe spectrometer (Thermo Fisher Scientific, Inc., Waltham, MA, USA) equipped with a microspot monochromatized Al Kα source.

Survey (binding energy range 0–1200 eV, pass energy 150 eV) and high resolution scans (pass energy 50 eV) were recorded in the FAT analyser mode.

Nonlinear least-squares curve fitting of the detailed spectra was performed by using the Avantage software package. Quantification was obtained by peak areas normalized by acquisition parameters and sensitivity factors provided by the manufacturer, whereas the binding energy (BE) scale was set by fixing the C1s component due to adventitious hydrocarbon at 285 eV (De Giglio, Cafagna, et al., 2011).

Before XPS analysis, all coatings were prepared by casting following the procedure reported above, while CIP powder was pressed onto a small square of double-stick carbon tape.

2.5. Ciprofloxacin determination by HPLC

High-performance liquid chromatography (HPLC) analyses of CIP were performed with an Agilent 1260 Infinity (Agilent Technologies, Santa Clara, CA), equipped with a MW detector, 20 μL

injection loop and processed by ChemStation for LC systems Agilent Technologies. For analysis, a reversed phase Synergy (15 cm × 4.6 mm; 4 μm particles; Phenomenex) column was eluted in isocratic mode using experimental conditions already reported (De Giglio, Cometa, et al., 2011).

2.6. Determination of ciprofloxacin content in the CSNPs

The Association Efficiency percentage (%AE) of CIP to the particles was calculated by an indirect method. CSNPs were isolated from unbound CIP by centrifugation (16,000 × g, 45 min, Eppendorf 5415D, Eppendorf, Germany), and free CIP in the supernatant was quantified by HPLC as described above. The %AE was calculated as follows (Eq. (1)):

$$\%AE = \frac{CIP_{tot} - CIP_{free}}{CIP_{tot}} \times 100 \quad (1)$$

where CIP_{tot} and CIP_{free} denote, respectively, the amounts of CIP present in the solution before and after the CIP-loaded CSNPs preparation.

2.7. Ciprofloxacin release studies

In vitro release studies of CIP were carried out on CIP-enriched CSNPs coatings up to 7 days at 37 °C. CIP-enriched CSNPs coated Ti sheets were dipped in 3.5 mL of physiological solution (NaCl 0.9%, w/v), under static conditions. At predetermined time intervals, an aliquot (200 μL) was withdrawn and CIP content was evaluated by HPLC as described above. A total volume of 3.5 mL was maintained by refilling 200 μL of the same medium after each withdrawal. All the experiments were done in triplicate.

2.8. Coatings antibacterial activity

Two clinical *S. aureus* strains, one biofilm producer and one not producer were used to test CIP-enriched CSNPs coating antibacterial activity. The two nosocomial strains were identified through biochemical tests performed by automated system Vitek2 (Biomerieux, France) using specific cards for Gram (+) bacteria. Before testing, Ti sheets coated with CIP-enriched CSNPs or unloaded CSNPs were sterilized by UV radiation (1 h/sheet side). The antibacterial activity protocol was carried out as described elsewhere (De Giglio et al., 2012). Briefly, a fresh culture on Mueller–Hinton agar plate was prepared for each isolate and one/two colonies from the culture were added to 2 mL of sterile water in order to have a 0.1 McFarland turbidity. 1 μL of this suspension was inoculated into 14 mL of Trypticase Soy Broth (obtaining 3×10^2 CFU/mL) (Akiyama et al., 2013; Bernthal et al., 2010). CIP-enriched CSNPs and unloaded CSNPs (used as control) titanium coatings were added to the suspension and incubated at 37 °C for 48 h. The total bacterial load (TBL) was determined by plating 1 mL of the suspension onto a sterile Petri dish, adding Nutrient Agar medium and incubating overnight at 37 °C. The number of CFU/mL was finally counted. Biofilm production was spectrophotometrically determined measuring bacterial biofilm optical density with a modified version of the polystyrene tissue culture plate test (Christensen et al., 1985).

2.9. Cell culture and viability

MG63 human osteoblast-like cells (ATCC, Rockville, MD, USA) were cultured onto the coated Ti sheets in 24-well polystyrene tissue culture plates (TCPs) at a density of 1×10^4 cells/cm^2 at 37 °C, as previously described (De Giglio et al., 2012). Before testing coated Ti specimens were UV sterilized (254 nm) for 1 h/sheet side. At 48 h, 7 and 14 days MTT (3-dimethylthiazol-2,5-diphenyltetrazolium bromide) colorimetric assay was performed according to manufacturer's instruction by a standard procedure (De Giglio, Cafagna, et al., 2011; De Giglio, Cometa, et al., 2011; De Giglio, Trapani, et al., 2011). Tests were performed in triplicate.

2.10. SEM morphological characterization

Cell culture specimens were examined using the secondary electron detector with a Philips XL 20 scanning electron microscope (FEI Europe Eindhoven, The Netherlands). For SEM analysis, samples were prepared as previously described (De Giglio, Cometa, et al., 2011). Observations of cells on CIP-enriched CSNPs coatings were compared with those on unloaded CSNPs coatings and on bare Ti sheets.

2.11. Fluorescence microscopy

Fluorescence staining for formation and reorganization of stress fibres and focal contacts was performed in cells cultured for 48 h and 7days. Itemized procedure can be found elsewhere (De Giglio, Cometa, et al., 2011). Briefly, cells were fixed with 4% paraformaldehyde (Sigma–Aldrich) in 0.1 M Phosphate-Buffered Saline (PBS), pH 7.4, at 4 °C for 30 min. Cells were permeabilized with 0.1% Triton X-100 (Sigma–Aldrich) in PBS 0.01 M to remove the nuclear envelope and soluble nuclear material, and then blocked with normal goat serum in PBS (dilution 1:5). Cells were incubated with FITC-labelled phalloidin (Sigma–Aldrich) (green fluorescence) 1:100 to visualize MG63 F-actin fibre organization, and with DAPI (Sigma–Aldrich) 1:1000, to stain cell nuclei, for 45 min at room temperature (RT). Images were photographed using a Zeiss AxioCam MRcs fluorescence microscope (Carl Zeiss Optical Inc., Germany) equipped with a Nikon DXM1200F Ultra High-Quality Digital Camera (NITAL S.p.A., Turin, Italy). Controls were represented by MG63 seeded (1×10^4cells/cm^2) onto bare Ti sheets. For analysis of the stress fibre formation, a five-point blind scoring system, measuring the degree of actin stress fibre was used (De Giglio, Cometa, et al., 2011; Tasi et al., 2004). Criteria scoring were the following: 1 = scarce or no resolved F-actin stress fibre formation and predominantly cortical actin; 2 = thin, short F-actin filament occupying at least 25% of the cell volume; 3 = modest stress fibre formation of F-actin where stress fibres are thicker and fill at least 50% of the cell volume; 4 = wide stress fibres formation where stress fibres are thick and well-defined, many traverse the full width of the cell; 5 = the whole cell is densely crammed with thick stress fibres, most traverse the width of the cell. At least 20 cells were counted for each substrate. Mean data ± SD are reported.

2.12. RNA extraction and reverse transcription

Total RNA was isolated from MG63 cultured onto titanium and CIP-enriched CSNPs coated titanium surfaces with Perfect Pure RNA Cultured Cell Kit (5-Prime GmbH, Hamburg, Germany) that provides DNase treatment, according to manufacturer's instructions. Quantification and evaluation of RNA quality were performed by spectrophotometric analysis (bioPhotometer plus, Eppendorf GmbH, Germany).

According to manufacturer's instructions, one microgram of total RNA was reverse transcribed in a 20 μL reaction volume using Masterscript RT-PCR System (Eppendorf GmbH) and oligo-(dt) primers (Jena Bioscience GmbH, Germany). Neo-synthesized cDNA was stored at −20 °C.

2.13. Real-time PCR assay

Real-time assays were performed by Mastercycler realplex2 (Eppendorf GmbH, Germany) using SsoFast™ EvaGreen®

Table 1
Analysed genes description (*reference gene).

Gene	Detected transcript	Primer forward (5′→3′)	Primer reverse (5′→3′)	Amplicon length (bp)	Annealing T (°C)
RUNX2	NM_004348.3	CTCGTCCGCACCGACAGCC	TACCTCTCCGAGGGCTACCACC	111	60
BMP2	NM_001200.2	CCAGCCGAGCCAACACTGTGC	TCTCCGGGTTGTTTTCCCACTCG	86	60
CDH11	NM_001797.2	CCGGAGTTCCTGCACGAGACCTA	TGGCGCTATTTCCATAAGTGGGGT	114	64
Type I collagen	NM_000088.3	GTGCTAAAGGTGCCAATGGT	CTCCTCGCTTTCCTTCCTCT	228	64
GAPDH*	NM_002046.3	AGCCACATCGCTCAGACAC	GCCCAATACGACCAAATCC	200	60

Supermix 1×, in a final volume of 10 μL. All PCR reactions contained 1 μL of cDNA (corresponding to 50 ng of total RNA template). Each PCR assay were performed in white plastic-ware and comprised 30 s at 95 °C for enzyme activation, 40 cycles of denaturation at 95 °C for 5 s, annealing and extension at 60 °C for 20 s. Every primers were used at 200 nM final concentration. Primers' sequences were designed by Primer 3 (v. 0.4.0) software. Their specificity was tested by BLAST Assembled RefSeq Genomes in order to avoid any appreciable homology to pseudogenes or other unexpected targets. In each assay, both reference gene and each gene of interest mRNA were measured simultaneously under identical conditions. Primers showed the same amplification efficiency. Specificity of the PCR reactions was furthermore confirmed by melt curve analysis. The oligonucleotide sequences for target genes are listed in Table 1.

2.14. Quantification of mRNA expression

Each assay was performed as triplicate and provide three references genes whose Cq values were used to normalize cellular mRNA data. In this instance normalization involved the ratio of mRNA concentrations of specific genes of interest (as mentioned above) to those of Cq medium value of the reference genes. In order to compare MG63 gene expression onto CIP-enriched CSNPs samples with untreated titanium surfaces, ΔΔCq method for the evaluation of Fold-Change was employed. Mean and standard deviation of three different experiments are reported. Data were analysed by one-way ANOVA, Student–Newman–Keuls's. Statistical significance was tested at $p < 0.05$.

3. Results and discussion

3.1. Physicochemical characterization of nanoparticles

Herein, for the first time, a nanoparticulate delivery system for CIP was proposed combining two cyclodextrins, namely SBE_{7m}-β-CD and γ-CD, which are both approved by FDA for parenteral administration. Moreover, due to their different chemical structure, in this work a particular strategy of nanoencapsulation was conceived: the negatively-charged SBE-β-CD crosslinked the positively-charged chitosan (Aresta et al., 2013) whereas the uncharged γ-CD was supposed to increase CIP loading in the chitosan network. Indeed, according to a previous study (Blanchemain et al., 2012), the larger cavity of γ-CD can efficiently host the guest molecule of CIP and, once an aliquot of the complex γ-CD/CIP was mixed with chitosan solution, the loading of the antibiotic in the chitosan network was enhanced. Table 2 summarized the physicochemical characteristics of nanoparticles: unloaded CSNPs had a particle size of 426 nm that slightly increase up to 552 nm in CIP-loaded CSNPs, probably since CIP was incorporated in the nanosystem. A high uniformity in particles size and morphology has been achieved, as suggested by PI values and TEM investigation. Both unloaded CSNPs and CIP-loaded CSNPs exhibited positive zeta potential values, according to the presence of externally located chitosan chains.

Table 2
Chemico-physical properties of unloaded chitosan nanoparticles (i.e. unloaded CSNPs) and ciprofloxacin-loaded chitosan nanoparticles (i.e. CIP-loaded CSNPs) (PI: polydispersity index; ζ: zeta potential; AE: association efficiency. Mean ± S.D. are reported, $n = 6$).

Formulation	Size (nm)	PI	ζ (mV)	AE (%)
Unloaded CSNPs	426 ± 14	0.24–0.27	+29.2 ± 0.7	–
CIP-loaded CSNPs	552 ± 26	0.25–0.34	+30.5 ± 0.7	71 ± 6

3.2. TEM characterization

TEM analysis showed single nanoparticles with an essential spherical structure in both unloaded CSNPs and CIP-loaded CSNPs, Fig. 1A and B, respectively. No massive agglomeration was evident. The higher diameter detected in CIP-loaded CSNPs versus unloaded CSNPs was probably related to the presence of ciprofloxacin as previously suggested (Krauland & Alonso, 2007).

3.3. XPS analysis

XPS analysis was employed to ascertain the surface chemical composition of the nanoparticle-based films casted on titanium. The presence of the antibiotic molecules in the coating was verified

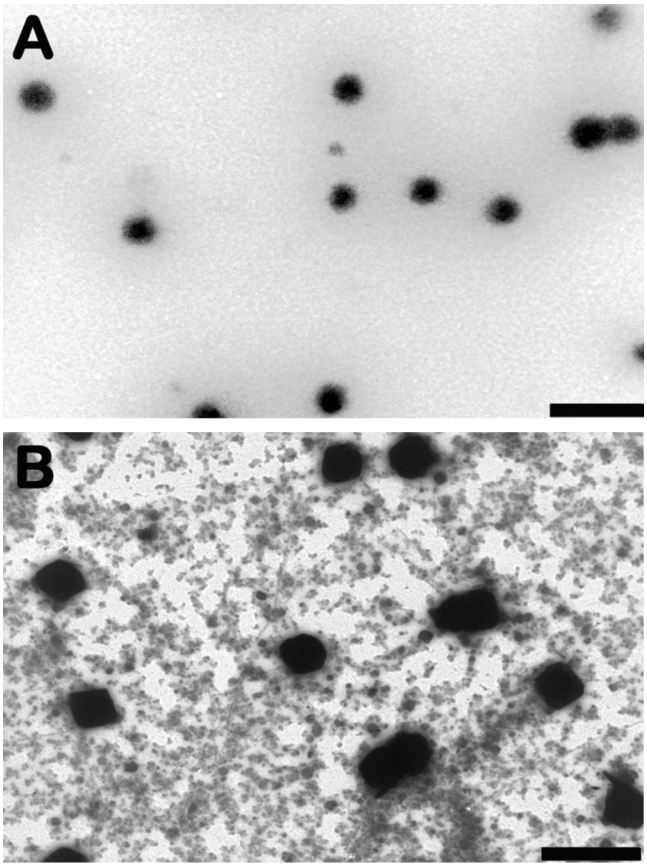

Fig. 1. TEM images of chitosan nanoparticles without CIP (i.e. unloaded CSNPs) (A) and with ciprofloxacin (i.e. CIP-loaded CSNPs) (B). Scale bars: 500 nm.

Table 3
Surface composition (i.e., atomic percentages obtained by XPS analysis) of ciprofloxacin (CIP), unloaded chitosan nanoparticles (i.e. unloaded CSNPs) and ciprofloxacin-enriched chitosan nanoparticles (i.e., CIP-enriched CSNPs).

Sample	Atomic percentage (%)						
	C	O	N	Cl	F	S	Na
CIP	70.4	11.6	11.3	3.1	3.5	–	–
Unloaded CSNPs	59.0	24.3	3.6	8.1	–	0.6	4.4
CIP-enriched CSNPs	66.6	17.5	4.4	6.1	1.1	0.9	3.5

by analysing XPS spectra of pure CIP compared with unloaded and CIP-enriched CSNPs samples.

The surface compositions of CIP, unloaded and CIP-enriched CSNPs samples, expressed as atomic percentages, were summarized in Table 3. In the case of CIP-loaded CSNPs samples, the XPS analysis revealed a surface composition almost similar to the unloaded CSNPs, evidencing a negligible surface presence of the incorporated antibiotic (data not shown).

Indeed, F1s signal is a clear marker of the presence of CIP on the surface of the proposed antibacterial formulation, since it was completely absent in the unloaded CSNPs spectrum. The fluorine binding energy (BE) at 687.3 eV was in good agreement with XPS literature data on structurally similar fluoroquinolones (Polishchuk, Karaseva, Emelina, Nikolenko, & Karasev, 2009).

As far as the N1s signals are concerned, the curve fitting relevant to CIP, unloaded and CIP-enriched CSNPs samples pointed out the presence of CIP in the latter nanoparticle system (Fig. 2). In particular, all the N1s signals have been deconvoluted into three peaks (identified as peak A, B and C in Fig. 2), whose relative amounts were different in the investigated samples (see Table 4). The peak A can be ascribed to aminic nitrogen but, at the same BE, a contribution from CIP piperazinic nitrogen can also be present in CIP and CIP-enriched CSNPs N1s spectra (Polishchuk et al., 2009). The peak B is attributed to amidic groups and, in CIP and CIP-enriched CSNPs samples, also to CIP nitrogen in 1,8-naphthiridine framework. Finally, the peak C arises from chitosan and/or CIP quaternary ammonium species. In the unloaded CSNPs the N1s was exclusively given by chitosan macromolecules. The atomic percentage of the component relevant to amide species (i.e. peak B in unloaded CSNPs) was in good agreement with the expected deacetylation degree of the pure chitosan employed. When CIP-enriched CSNPs system was examined, a significant enhancement of peak B was detected, due to the contribution of the naphthydrine nitrogen relevant to CIP molecules, indicating the external location of CIP, that could provide a first rapid availability of the antibiotic in the site of implantation.

3.4. Ciprofloxacin release from CIP-enriched CSNPs coatings on titanium substrates

Fig. 3 shows the release behaviour of CIP-enriched CSNPs coatings in physiological solution up to 7 days. CIP was rapidly released from the nanoparticle system over the first 6 h (approximately the 60% of the total amount released) and then a further slow release took place. The burst release from chitosan nanoparticles, already described for macromolecules like insulin and heparin (Krauland & Alonso, 2007) and for a complex β-cyclodextrin-CIP incorporated in the chitosan matrix (Chandran et al., 2010), could be ascribable either to the amount of CIP externally located (as evidenced by XPS data) or to the swelling of chitosan network. Even though a releasing profile comparable to that of our previous work, where the nanoparticle system was obtained using only SBE-β-CD (De Giglio et al., 2012), was detected, the introduction of γ-CD in the NPs formulation allowed a higher CIP amount deliverable. Taking into account the CIP enriched-CSNPs coating preparation procedure, about the 43% of the total CIP released raised from the adsorbed complex γ-CD/CIP, whereas the complementary moiety is related to the reservoir system constituted by the CIP-loaded

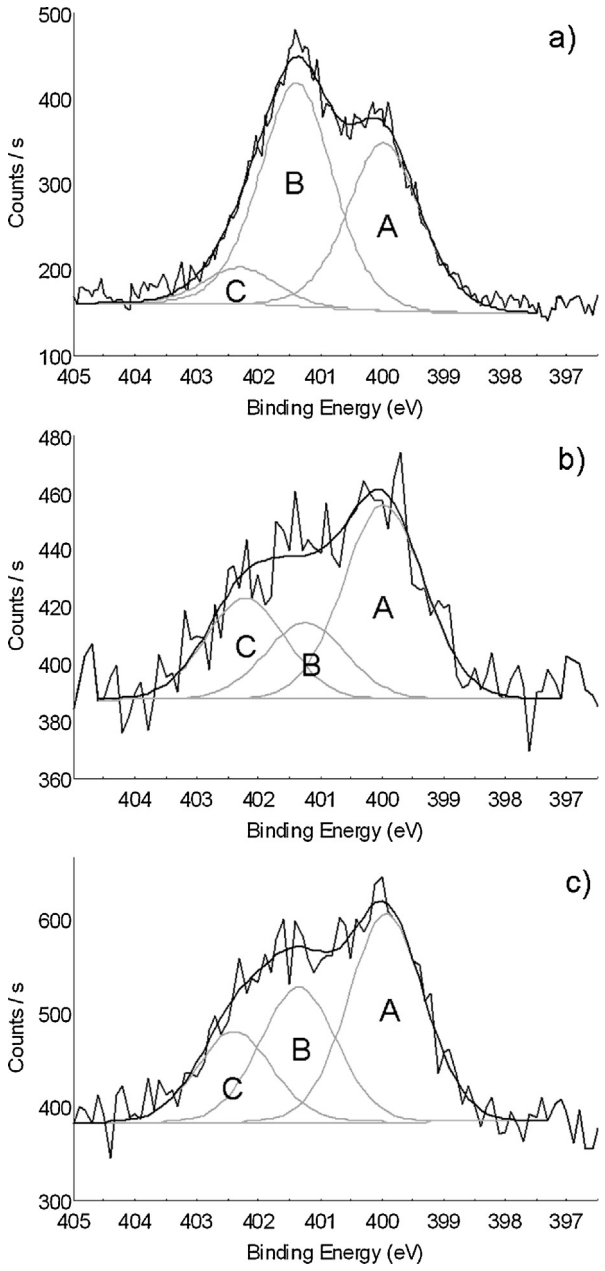

Fig. 2. XPS detailed spectra of N1s for ciprofloxacin (CIP) (a), unloaded chitosan nanoparticles (i.e., unloaded CSNPs) (b) and ciprofloxacin-enriched chitosan nanoparticles (i.e., CIP-enriched CSNPs) (c).

Table 4
Attributions, peaks position (BE) and relative atomic percentages (At%) of N1s peak components relevant to ciprofloxacin (CIP), unloaded chitosan nanoparticles (i.e. unloaded CSNPs) and ciprofloxacin-enriched chitosan nanoparticles (i.e. CIP-enriched CSNPs), shown in Fig. 3. The maximum error on the peak position is ±0.2 eV.

Attribution	BE (eV)	Atomic percentage (%)		
		CIP	Unloaded CSNPs	CIP-enriched CSNPs
A: N—H and/or piperazinic N	399.9	39.3	52.2	47.9
B: O=C—N and/or naphthydrine N	401.3	52.3	20.6	31.2
C: N^+—C	402.3	8.4	27.2	21.0

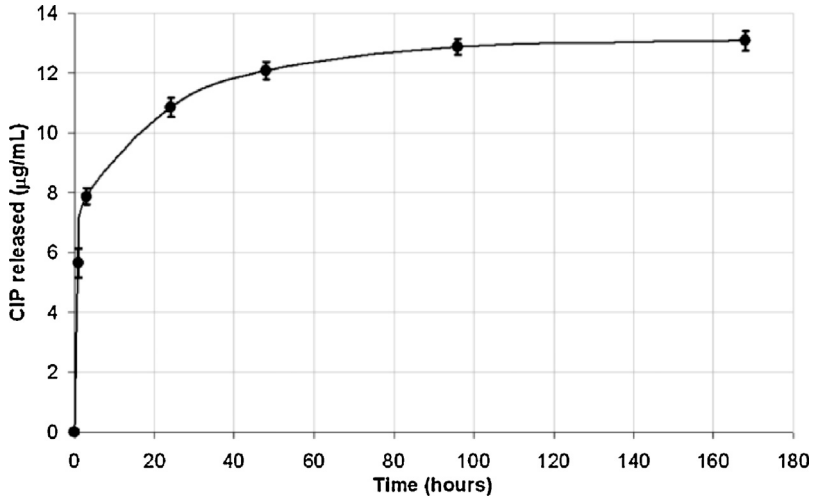

Fig. 3. Ciprofloxacin release from ciprofloxacin-enriched chitosan nanoparticles (i.e., CIP-enriched CSNPs) coatings on titanium substrates over time.

CSNPs. This feature represents an interesting improvement of the new investigated coating in comparison with our previous system, in which about the 77% of the total CIP released derived from the SBE-β-CD/CIP complex. Interestingly, the amount of CIP delivered once the plateau was reached (about 13 μg/mL) is much higher than minimal inhibitory concentration values (MIC ≤ 1 μg/mL) of two of the main pathogens involved in the orthopaedic infections as *S. aureus* and *P. aeruginosa*.

3.5. Antibacterial activity of CIP-enriched CSNPs coatings

The antibacterial activity of CIP-enriched CSNPs coatings against the two clinical strains of *S. aureus*, was verified. Fig. 4 showed that the proposed system inhibited the growth of the nosocomial *S. aureus* isolates during 48 h of observation. In particular, the presence of CIP-enriched CSNPs coatings decreased the bacterial growth about 20 times in comparison with control. On the other hand, the unloaded CSNPs coatings as well as titanium sheets, both used as control, did not produce any antibacterial effect. The curves of the two non-biofilm-forming and biofilm-forming *S. aureus* strains (Fig. 4a and b, respectively) indicated that the system was able to inhibit the growth of both isolates already from the first hours of incubation (see insets of Fig. 4) for almost 48 h (see Fig. 4), suggesting that the one biofilm producer was unable to synthesize extracellular matrix. This result is notably appealing, since staphylococcal-biofilm-associated infections result really hard to eradicate if not with the removal of the contaminated implant. The quick release of an appreciable amount of the antibiotic indicates the rapid efficacy of the coating against bacterial infections as well as its ability to inhibit the production of biofilm by microorganisms that are usually more resistant to antibiotics and human defence. In addition, the CIP-enriched CSNPs system inhibits the growth of the reference strains American Type Culture Collection (ATCC) 29213 *S. aureus* and ATCC 27853 *P. aeruginosa* (data not shown), suggesting that the system could be effective against either Gram (+) or Gram (−) bacteria.

3.6. Biocompatibility assessment

A serious concern on the use of local antibiotic therapy is related not only to the nature of the antibacterial agent but also to its concentration: a reduced drug release level (i.e. below MIC) is likely to evoke bacterial resistance (Stigter, Bezemer, de Groot, & Layrolle, 2004), whilst high doses may generate cell toxicity thus impairing osteogenic activity (Rathbone, Cross, Brown, Murray, & Wenke, 2011). In order to address the latter topic, we tested the effect of the CIP-enriched CSNPs coatings on metabolic activity, adhesion and gene expression of MG63 osteoblast-like cells comparing it with cell behaviour on unloaded CSNPs coatings and on bare Ti sheets. MG63 are relatively undifferentiated cells, phenotypically similar to mesenchymal progenitor cells and in culture behave as osteoblasts precursors (Lossdorfer et al., 2004; Reffitt et al., 2003). No significant differences in MTT test between unloaded CSNPs and CIP-enriched CSNPs coatings were detected at all-time point analysed. At 48 h values were higher than 70% (unloaded CSNPs

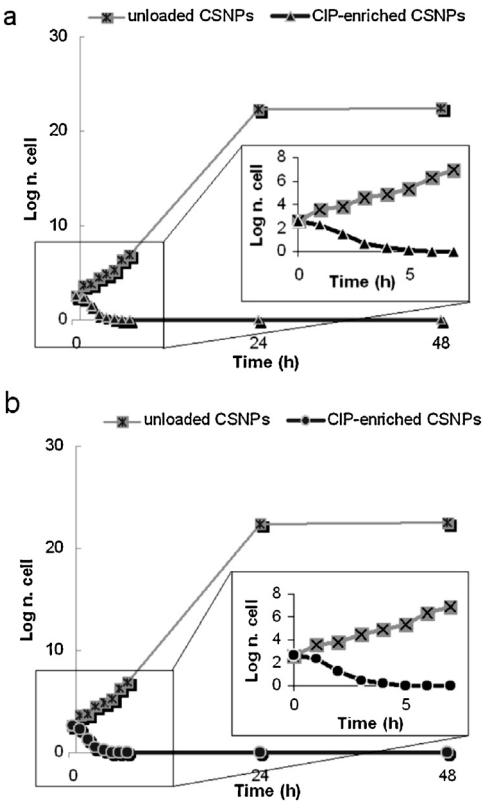

Fig. 4. Biofilm-forming (a) and non-biofilm-forming (b) *S. aureus* growth over time on unloaded chitosan nanoparticles (i.e. unloaded CSNPs) coatings, used as control, and ciprofloxacin-enriched chitosan nanoparticles (i.e., CIP-enriched CSNPs) coatings on titanium substrates. In the insets, details of the bacterial inhibition growth over the first 7 h were reported.

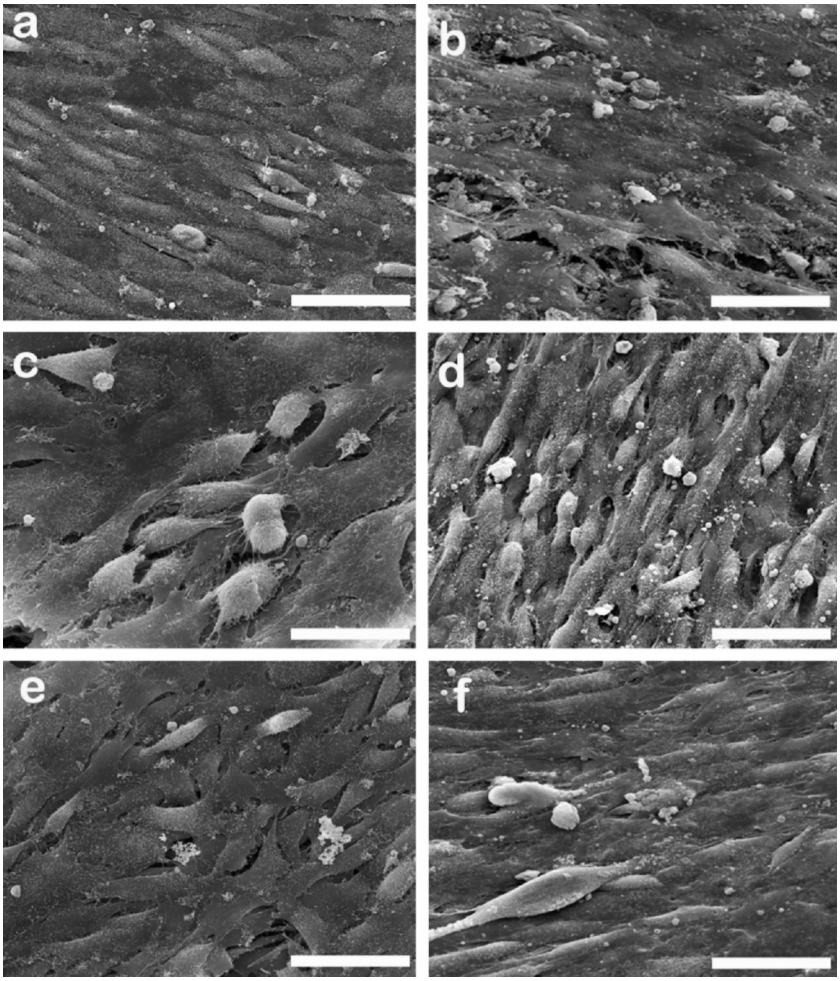

Fig. 5. SEM micrographs of MG63 cells cultured for 7 and 14 days on bare titanium sheets (a, b), chitosan nanoparticles (i.e. unloaded CSNPs) (c, d) and ciprofloxacin-enriched chitosan nanoparticles (i.e. CIP-enriched CSNPs) coatings (e, f). Scale bars = 50 μm.

77 ± 3%; CIP-enriched CSNPs 74 ± 2%) and increased up to 90% after 14 days of culture (unloaded CSNPs 95 ± 4%; CIP-enriched CSNPs 90 ± 5%).

MTT data were confirmed by SEM morphological observations at 7 and 14 days. At 7 days most MG63 cells grown on bare Ti sheets (Fig. 5a) displayed an elongated morphology, whereas on unloaded CSNPs coatings (Fig. 5c) and on CIP-enriched CSNPs coatings (Fig. 5e) they appeared more spread, as in activated osteoblasts. At 14 days a homogeneous distribution and the typical star-shaped cell morphology were observed on all investigated samples (Fig. 5b, d and f).

In order to further assess changes in cell adhesion and spreading of MG63 osteoblast-like cells seeded onto the tested coatings, phalloidin staining for actin filament was used. Cell cytoskeletal organization, detected at 48 h and 7 days on the unloaded CSNPs and CIP-enriched CSNPs coatings, was compared with the ones of MG63 cultured on bare Ti sheets (Table 5). In the latter specimens an elevated cell density with evident focal contact was present at 48 h; after 7 days of culture cells displayed a well-defined cytoskeletal organization and many stress fibres (score 3.8 ± 0.9) (Fig. 6a, d). Rounded cells with tight filopodia and cells displaying an organized sub-cortical F-actin cytoskeleton were present on unloaded CSNPs coatings at 48 h of culture, while an increase in cell density as well as in stress fibres formation was detected at 7days (Fig. 6b, e). Cells cultured on CIP-enriched CSNPs coating displayed at 48 h a star-shaped morphology with many focal contacts and with stress fibres filling at least the 25% of cell volume; at 7 days of culture MG63 cytoskeletal organization was equivalent to the other experimental conditions (Fig. 7c, f).

Table 5
Results of the analysis of the stress fibre formation on the different substrates with a five-point blind scoring system, measuring the degree of actin stress fibre (see Section 2). Mean data ± SD are reported.

	48 h	7days
Bare Ti	3.2 ± 0.7	3.8 ± 0.9
Unloaded CSNPs	1.8 ± 0.7	3.3 ± 0.8
CIP-loaded CSNPs	2.6 ± 0.5	3.4 ± 1.0

The grade of osteoblasts bonding and spreading to a biomaterial will affect their proliferation, differentiation as well as osseointegration at the implant site (Reyes, Petrie, Burns, Schwartz, & García, 2007). Indeed, osteoblasts differentiation and subsequent bone formation is a well-orchestrated and gradual process that involves changes in gene expression over time and it is characterized, in vitro, by three developmental stages: proliferation, extracellular matrix production and matrix mineralization (Isaac et al., 2010). To evaluate if and how CIP release could affect MG63 cells performance, mRNA levels of genes expressed during the early phases of osteoblast differentiation (i.e. runx2, bmp2, OB-cadherin, and collagen-type I) as well as of osteocalcin (bglap) that is transcribed later were determined using real time PCR (qRT-PCR), at 7 and 14 days of culture. We detected that these

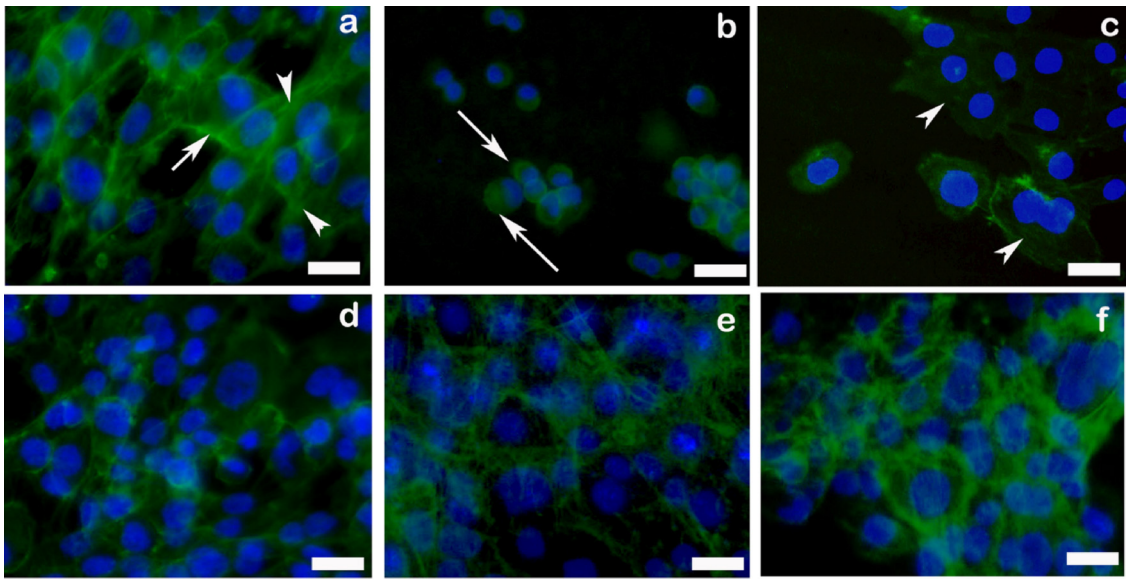

Fig. 6. Fluorescence detection of F-actin stress fibres in MG63 cultured on bare titanium sheets (a–d), on unloaded chitosan nanoparticles (i.e. unloaded CSNPs) (b–e) and ciprofloxacin-enriched chitosan nanoparticles (i.e. CIP-enriched CSNPs) coatings (c–f). At 48 h, evident focal contacts (arrows) and cytoplasm stress fibres (pointed arrow) were present on the titanium controls (a); on unloaded CSNPs coatings (b) cells were rounded and displayed an organized sub-cortical F-actin cytoskeleton (arrow); (c) cells cultured on CIP-enriched CSNPs coatings displayed a star-shaped morphology with stress fibres (pointed arrows) occupying at least the 25% of adhering cell volume. At 7 days, cytoskeletal organization was comparable in cells cultured on titanium sheet (d), on unloaded CSNPs (e) and on CIP-enriched CSNPs (f) coatings. Scale bars 20 μm.

selected genes were present through the culture period but they showed a different expression pattern over time (Fig. 7), with major changes for runx2 and bmp2. Runx2 is one of the first transcription factor required for the determination of the osteoblast lineage (Reyes et al., 2007); normally, the protein level of runx2 is reduced in osteoblasts during bone development and when osteoblasts acquire a mature phenotype. The comparison of cells seeded onto CIP-enriched CSNPs coating with those seeded on unloaded CSNPs coating evidenced a significant increase after 7 days of culture, while after 14 days its expression was only slightly raised. A similar pattern was seen for bmp2, which is a potent local regulator of osteoblast differentiation (Yamaguchi, Komori, & Suda, 2000) and is controlled by runx2. Bmp2 has an increase in its expression after 7 days of culture in MG63 seeded onto CIP-enriched CSNPs

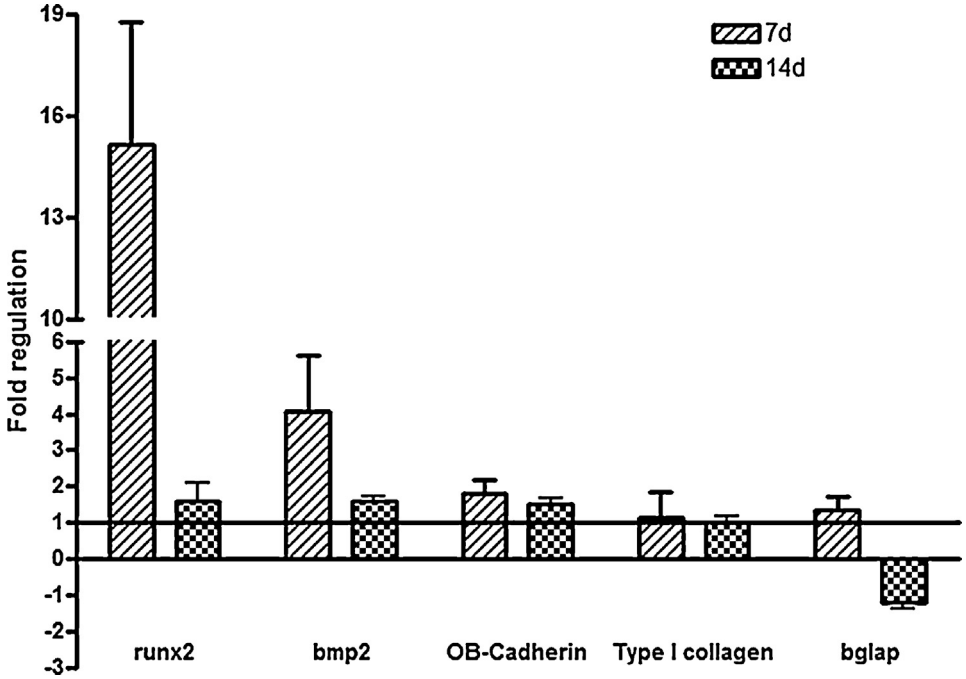

Fig. 7. qRT-PCR gene expression of runx2, bmp2, OB-cadherin, collagen-type I and osteocalcin (bglap) in MG63 seeded onto ciprofloxacin-enriched chitosan nanoparticles (i.e., CIP-enriched CSNPs) coatings in comparison with those seeded on unloaded chitosan nanoparticles (i.e. unloaded CSNPs) coatings. For bare titanium sheets fold-change was 1 (continuous line). Data are expressed as Fold-regulation that represents fold-change results in a biologically expressive manner. Fold-regulation is equal to the fold-change ($2^{(-\Delta\Delta Ct)}$) for fold-change values greater than one and indicate an up-regulation. Fold-change values less than one indicate a down-regulation; in this case the fold-regulation is the negative inverse of the fold-change.

coatings in comparison with those seeded on unloaded CSNPs coatings, while a modest increment was detected after 14 days of culture. This behaviour is consistent with the bmp2 induction by runx2. On the contrary, no significant changes in OB-cadherin, collagen-type I, and osteocalcin expression were detected between cells seeded onto CIP-enriched CSNPs coatings and those seeded on unloaded CSNPs coatings after 7 days of culture, with a fold regulation equal to 1 that is the normal fold regulation in control (i.e. cells seeded onto unloaded CSNPs). OB-cadherin has a multifunctional role in the skeletal system and it contributes to postnatal skeletal growth and to the acquisition of normal bone mass, microarchitecture and strength (Di Benedetto et al., 2010). Moreover it interacts with β-catenin and plakoglobin in the adherence junction, and β-catenin also serves as transcription factor for osteogenic commitment, since cell-cell as well as cell-material adhesions are disrupted by cadherin deficiency in osteoblasts (Di Benedetto et al., 2010). The qRT-PCR data on its expression confirmed the morphological observation of a good cell adhesion on CIP-enriched CSNPs coatings. The unchanged collagen-type I expression suggested that the presence and/or release of CIP from the coating did not alter one of the main indicator of bone matrix synthesis. At last, as far as mRNA osteocalcin expression is concerned, unmodified expression on this gene was detected after 7 days of culture, while after 14 days a reduction was observed. Two could be the reasons for this observation: the reduction could be at least in part related to the increase in cell proliferation rate experienced at the same time point or MG63 need the presence of specific growth factors able to promote their further differentiation (i.e. osteocalcin expression). As a whole, these data pointed out that the developed CIP-enriched CSNPs coatings owning antibacterial activity, do not affect osteoblast-like cells proliferation and differentiation.

4. Conclusions

In the present work a new antibiotic-loaded chitosan nanoparticle coating for titanium implants was proposed as an efficient vehicle for ciprofloxacin in situ delivery. The main novelty of this system is the combination of SBE_{7m}-β-CD (acting as counterion towards chitosan) and γ-CD (able to efficiently incorporate the antibiotic) in the drug delivery system formulation. To gain insight into the surface composition of the nanosized system, size distribution and morphological features, XPS and TEM analyses were performed. Ciprofloxacin release was also evaluated. The resulting coating exhibited a strong antibacterial efficacy against nosocomial strains of *S. aureus* (either biofilm producer or not), inhibiting the growth of both isolates already from the first hours of incubation. Moreover, the proposed nanosized coating do not affect MG63 osteoblast-like cells proliferation, adhesion and gene expression up to 14 days. Hence, this new nanoparticle-based coating capable to reduce bacterial infection not jeopardizing osseointegration can be considered a promising biocompatible drug delivery system for orthopaedic or dental surgery applications.

Acknowledgements

This project was supported by Università degli Studi di Bari Aldo Moro (FAR to E. De Giglio) and by FIRB (RBAP10MLK7) and PRIN (2010J8RYS7) project grants (Università Politecnica delle Marche). We acknowledge Dr. Gabriella Teti (University of Bologna) and Dr. Raffaella Lazzarini (Università Politecnica delle Marche) for their helpful technical support in TEM analysis and biomolecular studies, respectively.

References

Agnihotri, S. A., Mallikarjuna, N. N., & Aminabhavi, T. M. (2004). Recent advances on chitosan-based micro- and nanoparticles in drug delivery. *Journal of Controlled Release*, *100*, 5–28.

Akiyama, T., Miyamoto, H., Yonekura, Y., Tsukamoto, M., Ando, M., Noda, I., et al. (2013). Silver oxide-containing hydroxyapatite coating has in vivo antibacterial activity in the rat tibia. *Journal of Orthopaedic Research*, *31*, 1195–1200.

Amaral, I. F., Sampaio, P., & Barbosa, M. A. (2006). Three-dimensional culture of human osteoblastic cells in chitosan sponges: The effect of the degree of acetylation. *Journal of Biomedical Materials Research*, *76A*, 335–346.

Aresta, A., Calvano, C., Trapani, A., Cellamare, S., Zambonin, C. G., & De Giglio, E. (2013). Development and analytical characterization of vitamin(s)-loaded chitosan nanoparticles for potential food packaging applications. *Journal of Nanoparticle Research*, *15*, 1592–1603.

Bernthal, N. M., Stavrakis, A. I., Billi, F., Cho, J. S., Kremen, Y. J., Simon, S. I., et al. (2010). A mouse model of post-arthroplasty *Staphylococcus aureus* joint infection to evaluate in vivo the efficacy of antimicrobial implant coatings. *PLoS One*, *5*(9), e12580, 1–11

Blanchemain, N., Karrout, Y., Tabary, N., Neut, C., Bria, M., Siepmann, J., et al. (2011). Methyl-β-cyclodextrin modified vascular prosthesis: Influence of the modification level on the drug delivery properties in different media. *Acta Biomaterialia*, *7*, 304–314.

Blanchemain, N., Karrout, Y., Tabary, N., Bria, M., Neut, C., Hildebrand, H. F., et al. (2012). Comparative study of vascular prostheses coated with polycyclodextrins for controlled ciprofloxacin release. *Carbohydrate Polymers*, *90*, 1695–1703.

Brohede, U., Forsgren, J., Roos, S., Mihranyan, A., Engqvist, H., & Strømme, M. (2009). Multifunctional implant coatings providing possibilities for fast antibiotics loading with subsequent slow release. *Journal of Materials Science: Materials in Medicine*, *20*, 1859–1867.

Buchholz, H. W., & Engelbrecht, H. (1970). Depot effects of various antibiotics mixed with Palacos resins. *Der Chirurg*, *41*, 511–515.

Bumgardner, J. D., Wiser, R., Gerard, P. D., Bergin, P., Chestnutt, B., Marin, M., et al. (2003). Chitosan: Potential use as a bioactive coating for orthopaedic and craniofacial/dental implants. *Journal of Biomaterials Science, Polymers*, *14*, 423–438.

Busilacchi, A., Gigante, A., Mattioli-Belmonte, M., Manzotti, S., & Muzzarelli, R. A. A. (2013). Chitosan stabilizes platelet growth factors and helps modulate stem cell differentiation for tissue regeneration. *Carbohydrate Polymers*, *98*, 665–676.

Chandran, S. C., Shirwaikar, A., Sarala, A., & Devi Kiron, S. S. (2010). Development and evaluation of chitosan ocuserts containing ciprofloxacin and β-CD complex. *International Journal of PharmTech Research*, 246–252.

Christensen, G. D., Simpson, W. A., Younger, J. J., Baddour, L. M., Barrett, F. F., Melton, D. M., et al. (1985). Adherence of coagulase-negative staphylococci to plastic tissue culture plates: A quantitative model for the adherence of staphylococci to medical devices. *Journal of Clinical Microbiology*, *6*, 996–1006.

Cometa, S., Iatta, R., Ricci, M. A., Ferretti, C., & De Giglio, E. (2013). Analytical characterization and antimicrobial properties of novel copper nanoparticle-loaded electrosynthesized hydrogel coating. *Journal of Bioactive and Compatible Polymers*, *28*, 508–522.

Cooke, E. M., Coello, R., Sedgwick, J., Ward, V., Wilson, J., Charlett, A. B., et al. (2000). A national surveillance scheme for hospital associated infections in England Team of the Nosocomial Infection National Surveillance Scheme. *Journal of Hospital Infections*, *46*, 1–3.

De Giglio, E., Cometa, S., Satriano, C., Sabbatini, L., & Zambonin, P. G. (2009). Electrosynthesis of hydrogel films on metal substrates for the development of coatings with tunable drug delivery performances. *Journal of Biomedical Materials Research A*, *88*.

De Giglio, E., Cometa, S., Ricci, M. A., Zizzi, A., Cafagna, D., Manzotti, S., et al. (2010). Development and characterization of rhVEGF-loaded poly(HEMA-MOEP) coatings electrosynthesised on titanium to enhance bone mineralization and angiogenesis. *Acta Biomaterialia*, *6*, 282–290.

De Giglio, E., Cafagna, D., Giangregorio, M. M., Domingos, M., Mattioli-Belmonte, M., & Cometa, S. (2011). PHEMA-based thin hydrogel films for biomedical application. *Journal of Bioactive and Compatible Polymers*, *26*, 420–434.

De Giglio, E., Cometa, S., Ricci, M. A., Cafagna, D., Savino, A. M., Sabbatini, L., et al. (2011). Ciprofloxacin-modified electrosynthesized hydrogel coatings to prevent titanium-implant-associated infections. *Acta Biomaterialia*, *7*, 882–891.

De Giglio, E., Trapani, A., Cafagna, D., Sabbatini, L., & Cometa, S. (2011). Dopamine-loaded chitosan nanoparticles: Formulation and analytical characterization. *Analytical and Bioanalytical Chemistry*, *400*, 1997–2002.

De Giglio, E., Trapani, A., Cafagna, D., Ferretti, C., Iatta, R., Cometa, S., et al. (2012). Ciprofloxacin-loaded chitosan nanoparticles as titanium coatings: A valuable strategy to prevent implant-associated infections. *Nano Biomedicine and Engineering*, *4*, 163–169.

De Giglio, E., Cafagna, D., Cometa, S., Allegretta, A., Pedico, A., Giannossa, L. C., et al. (2013). An innovative, easily fabricated, silver nanoparticle-based titanium implant coating: Development and analytical characterization. *Analytical and Bioanalytical Chemistry*, *405*, 805–816.

Di Benedetto, A., Watkins, M., Grimston, S., Salazar, V., Donsante, C., Mbalaviele, G., et al. (2010). N-cadherin and cadherin 11 modulate postnatal bone growth and osteoblast differentiation by distinct mechanisms. *Journal of Cell Science*, *123*, 2640–2648.

Giammona, G., Pitarresi, G., Palumbo, F., Romano, C. L., Meani, E., & Cremascoli, E. (2010). *Antibacterial hydrogel and use thereof in orthopedics* (US Patent 0280921, November 17).

Gollwitzer, H., Ibrahim, K., Meyer, H., Mittelmeier, W., Busch, R., & Stemberger, A. (2003). Antibacterial poly(D,L-lactic acid) coating of medical implants using a biodegradable drug delivery technology. *Journal of Antimicrobial Chemotherapy*, *51*, 585–591.

Heinemann, C., Heinemann, S., Bernhardt, A., Worch, H., & Hanke, T. (2008). Novel textile chitosan scaffolds promote spreading, proliferation, and differentiation of osteoblasts. *Biomacromolecules*, *9*.

Herbold, B. A., Brendler-Schwaab, S. Y., & Ahr, H. J. (2001). Ciprofloxacin: In vivo genotoxicity studies. *Mutation Research*, *498*, 193–205.

Isaac, J., Galtayries, A., Kizuki, T., Kokubo, T., Berda, A., & Sautier, J. M. (2010). Bioengineered titanium surfaces affect the gene-expression and phenotypic response of osteoprogenitor cells derived from mouse calvarial bones. *European Cells and Materials*, *20*, 178–196.

Jose, B., Antoci, V., Jr., Zeiger, A. R., Wickstrom, E., & Hickok, N. J. (2005). Vancomycin covalently bonded to titanium beads kills *Staphylococcus aureus*. *Chemistry and Biology*, *12*.

Krauland, H. A., & Alonso, M. J. (2007). Chitosan/cyclodextrin nanoparticles as macromolecular drug delivery system. *International Journal of Pharmaceutics*, *340*, 134–142.

Lahiji, A., Sohrabi, A., Hungerford, D. S., & Frondoza, C. G. (2000). Chitosan supports the expression of extracellular matrix proteins in human osteoblasts and chondrocytes. *Journal of Biomedical Materials Research*, *51*, 586–595.

Li, H., Ogle, H., Jiang, B., Hagar, M., & Li, B. (2010). Cefazolin embedded biodegradable polypeptide nanofilms promising for infection prevention: a preliminary study on cell responses. *Journal of Orthopaedic Research*, *28*, 979–1118.

Lossdorfer, S., Schwartz, Z., Lohmann, C. H., Greenspan, D. C., Ranly, D. M., & Boyan, B. D. (2004). Osteoblast response to bioactive glasses in vitro correlates with inorganic phosphate content. *Biomaterials*, *25*, 2547–2555.

Lucke, M., Schmidmaier, G., Sadoni, S., Wildemann, B., Schiller, R., Haas, N. P., et al. (2003). Gentamicin coating of metallic implants reduces implant-related osteomyelitis in rats. *Bone*, *32*, 521–531.

Mattioli-Belmonte, M., Orciani, M., Ferretti, C., Orsini, G., De Giglio, E., & Di Primio, R. (2010). Cell behaviour on bioactive polymeric coatings. *Italian journal of anatomy and embryology*, *115*, 127–133.

Motwani, S. K., Chopra, S., Talegaonkar, S., Kohli, K., Ahmad, F. J., & Khar, R. K. (2008). Chitosan-sodium alginate nanoparticles as submicroscopic reservoirs for ocular delivery: Formulation, optimisation and in vitro characterization. *European Journal of Pharmaceutics and Biopharmaceutics*, *68*, 513–525.

Noreen, J., Hickok, I., & Shapiro, M. (2012). Immobilized antibiotics to prevent orthopaedic implant infections. *Advanced Drug Delivery Review*, *64*, 1165–1176.

Park, J. H., Saravanakumar, G., Kim, K., & Kwon, I. C. (2010). Targeted delivery of low molecular drugs using chitosan and its derivatives. *Advanced Drug Delivery Review*, *62*, 28–41.

Paul, W., & Sharma, C. P. (2000). Chitosan, a drug carrier for the 21st century: A review. *STP Pharma Sciences*, *10*, 5–22.

Polishchuk, A. V., Karaseva, É. T., Emelina, T. B., Nikolenko, Y. M., & Karasev, V. E. (2009). Electronic structure and spectroscopic properties of norfloxacin, enoxacin, and nalidixic acid. *Journal of Structural Chemistry*, *50*, 434–438.

Rathbone, C. R., Cross, J. D., Brown, K. V., Murray, C. K., & Wenke, J. C. (2011). Effect of various concentrations of antibiotics on osteogenic cell viability and activity. *Journal of Orthopedic Research*, *29*, 1070–1074.

Reffitt, D. M., Ogston, N., Jugdaohsingh, R., Cheung, H. F., Evans, B. A., Thompson, R. P., et al. (2003). Orthosilicic acid stimulates collagen type 1 synthesis and osteoblastic differentiation in human osteoblast-like cells in vitro. *Bone*, *32*, 127–135.

Reyes, C. D., Petrie, T. A., Burns, K. L., Schwartz, Z., & García, A. J. (2007). Biomolecular surface coating to enhance orthopaedic tissue healing and integration. *Biomaterials*, *28*, 3228–3235.

Romano, C. L., Giammona, G., Giardino, R., & Meani, E. (2011). Antibiotic-loaded resorbable hydrogel coating for infection prophylaxis of orthopaedic implants, preliminary studies. *The Journal of Bone and Joint Surgery. British Volume*, *93-B*(Suppl. III), 337–338.

Sansone, J. M., Wilsman, N. J., Leiferman, E. M., Conway, J., Hutson, P., & Noonan, K. J. (2009). The effect of fluoroquinolone antibiotics on growing cartilage in the lamb model. *Journal of Pediatric Orthopaedic*, *29*(2), 189–195.

Stigter, M., Bezemer, J., de Groot, K., & Layrolle, P. (2004). Incorporation of different antibiotics into carbonated hydroxyapatite coatings on titanium implants, release and antibiotic efficacy. *Journal of Controlled Release*, *99*, 127–137.

Tasi, I. Y., Kimura, M., Stockton, R., Green, J. A., Puig, R., Jacobson, B., et al. (2004). Fibroblast adhesion to micro- and nano-heterogeneous topography using diblock copolymers and homopolymers. *Journal of Biomedical Materials Research*, *71*, 462–469.

Thatte, H. S., Zagarins, S., Khuri, S. F., & Fischer, T. H. (2004). Mechanisms of poly-N-acetyl glucosamine polymer-mediated hemostasis: Platelet interactions. *Journal of Trauma*, *57*, S13–S21.

Trapani, A., De Giglio, E., Cafagna, D., Denora, N., Agrimi, G., Cassano, T., et al. (2011). Characterization and evaluation of chitosan nanoparticles for dopamine brain delivery. *International Journal of Pharmaceutics*, *419*, 296–307.

Ventura, C. A., Tommasini, S., Crupi, E., Giannone, I., Cardile, V., & Musumeci, T. (2008). Chitosan microspheres for intrapulmonary administration of moxifloxacin: Interaction with biomembrane models and in vitro permeation studies. *European Journal of Pharmaceutics and Biopharmaceutics*, *68*, 235–244.

Ventura, C. A., Cannavà, C., Stancanelli, R., Paolino, D., Cosco, D., La Mantia, A., et al. (2011). Gemcitabine-loaded chitosan microspheres. Characterization and biological in vitro evaluation. *Biomedical Microdevices*, *13*, 799–807.

Yamaguchi, A., Komori, T., & Suda, T. (2000). Regulation of osteoblast differentiation mediated by bone morphogenetic proteins, hedgehogs, and Cbfa1. *Endocrine Reviews*, *21*, 393–411.